Annals of Biomedical Engineering, Vol. 39, No. 6, June 2011 (© 2011) pp. 1690–1702
DOI: 10.1007/s10439-011-0272-y

Characterization of Mitral Valve Annular Dynamics in the Beating Heart

MANUEL K. RAUSCH,[1] WOLFGANG BOTHE,[3] JOHN-PEDER ESCOBAR KVITTING,[3] JULIA C. SWANSON,[3] NEIL B. INGELS JR.,[3,4] D. CRAIG MILLER,[3] and ELLEN KUHL[1,2,3]

[1]Department of Mechanical Engineering, Stanford University School of Engineering, Stanford, CA, USA; [2]Department of Bioengineering, Stanford University School of Engineering, Stanford, CA, USA; [3]Department of Cardiothoracic Surgery, Stanford University School of Medicine, Stanford, CA, USA; and [4]Department of Cardiovascular Physiology and Biophysics, Palo Alto Medical Foundation, Palo Alto, CA, USA

(*Received 15 November 2010; accepted 4 February 2011; published online 19 February 2011*)

Associate Editor Jane Grande-Allen oversaw the review of this article.

Abstract—The objective of this study is to establish a mathematical characterization of the mitral valve annulus that allows a precise qualitative and quantitative assessment of annular dynamics in the beating heart. We define annular geometry through 16 miniature markers sewn onto the annuli of 55 sheep. Using biplane videofluoroscopy, we record marker coordinates *in vivo*. By approximating these 16 marker coordinates through piecewise cubic splines, we generate a smooth mathematical representation of the 55 mitral annuli. We time-align these 55 annulus representations with respect to characteristic hemodynamic time points to generate an averaged baseline annulus representation. To characterize annular physiology, we extract classical clinical metrics of annular form and function throughout the cardiac cycle. To characterize annular dynamics, we calculate displacements, strains, and curvature from the discrete mathematical representations. To illustrate potential future applications of this approach, we create rapid prototypes of the averaged mitral annulus at characteristic hemodynamic time points. In summary, this study introduces a novel mathematical model that allows us to identify temporal, regional, and inter-subject variations of clinical and mechanical metrics that characterize mitral annular form and function. Ultimately, this model can serve as a valuable tool to optimize both surgical and interventional approaches that aim at restoring mitral valve competence.

Keywords—Mitral regurgitation, Mitral valve, Annulus, Dynamics, Strain, Curvature, Splines.

INTRODUCTION

Mitral regurgitation is a common form of valvular heart disease affecting more than 2.5 million people in the United States, a number that is expected to double by 2030 as the population ages and grows.[15] Annually, more than 300,000 people worldwide, 44,000 in the United States alone, undergo open heart surgery for mitral valve treatment.[2] Mitral annuloplasty is the most common surgical procedure to repair a leaking valve.[40] The rationale behind mitral annuloplasty is to optimize annular dimensions and shape. However, despite intense research within the past decades, the classification of different repair techniques and devices remains largely qualitative. To optimize treatment strategies for mitral regurgitation, it is crucial to thoroughly understand normal mitral annular dynamics, in particular, to identify extreme values of strain and curvature, and the locations at which they occur. The objective of this study is to establish a mathematical characterization of the mitral valve annulus that allows a precise qualitative and quantitative assessment of annular dynamics in the beating heart. We hypothesize that clinical and mechanical metrics of annular form and function display significant temporal, regional, and inter-subject variations. We will test this hypothesis by adopting a hybrid experimental/computational approach combining an ovine model of normal healthy hearts, an imaging technique based on videofluoroscopic markers and a computational reconstruction of the mitral annulus using the field theories of continuum mechanics.

The mitral annulus is defined as the transitional region between the atrial myocardium and the mitral valve leaflet tissue. It is subdivided into lateral and septal portions that are separated by the trigones.[41,49] While the lateral annulus is considered muscular and flexible, its counterpart is known to be fibrous and rather stiff. The shape of the mitral annulus has been

Address correspondence to Ellen Kuhl, Department of Mechanical Engineering, Stanford University School of Engineering, Stanford, CA, USA. Electronic mail: ekuhl@stanford.edu

described as the border of a hyperbolic paraboloid with an elliptical two-dimensional (2D) projection. Due to its resemblance with a saddle, the mitral annulus has also been called saddle shaped.[23,37,38] Its highpoints are close to the mid-septal and mid-lateral sections (SEP and LAT, respectively, Fig. 1); its low points at the antero-lateral and the postero-medial commissures (AC and PC, respectively, Fig. 1). In a series of experimental and computational studies, this particular shape has been associated with an optimal stress distribution over the mitral valve leaflet.[22,42,45] Numerous studies proved the mitral annulus to undergo complex three-dimensional (3D) deformation throughout the cardiac cycle with characteristic changes in its geometric parameters including saddle height (SH), septal-lateral diameter, commissure–commissure diameter, and mitral annular area (MAA).[18,48,51] Shape, size, and dynamics of the mitral annulus are closely related to mitral valve function; deviations from the normal have been associated with mitral valve insufficiency. Typical examples of pathologies that affect mitral annular shape and kinematics are ischemic and dilated cardiomyopathy.[33]

During the past decades, surgical repair techniques and medical devices have been developed that share the ultimate goal of restoring mitral valve function without valve replacement.[7,8] Ideally, such surgical interventions reconstruct the native mitral valve apparatus while maintaining its dynamic character.[27] In order to do so, however, a comprehensive baseline database must be established that, among other parameters, reports on normal mitral annular dynamics. Earlier studies have reported on the dynamic changes of the mitral annulus in humans as well as in animals using echocardiography,[1,26] sonocrystal tracking,[20] and biplane videofluoroscopy.[39] Unfortunately, most of these studies are based on a small numbers of study subjects and have a low temporal or spatial resolution. Moreover, most existing studies focus exclusively on the clinical characterization of the mitral annulus neglecting the mechanical characterization necessary to fully comprehend mitral annular dynamics. The goal of this study is therefore to use our well-documented method of tracking implanted miniature markers over the cardiac cycle in the beating heart[5,6,11] to identify temporal, regional, and inter-subject variations of clinical and mechanical metrics to characterize mitral annular form and function in the normal beating heart.

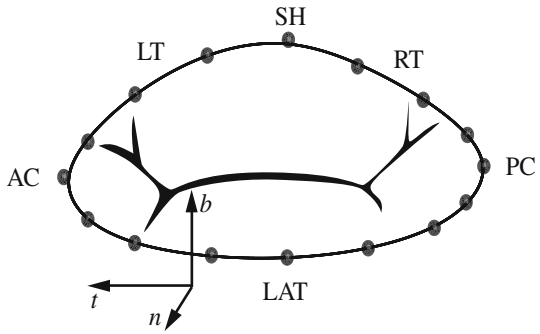

FIGURE 1. Schematic of mitral valve annulus created from piecewise cubic splines c(*s*, *t*) (black curve) fitted through *n* = 1,...,16 implanted miniature markers (black spheres). A local coordinate system can be defined at each point in time *t* along the curve c for discrete arc length parameters 0 ≤ *s* ≤ 1 through the tangential vector t, the normal vector n, and the binormal vector b. AC: antero-lateral commissure, PC: postero-medial commissure, SEP: septal annulus, LAT: lateral annulus, LT: left trigone, RT: right trigone.

To compute relevant characteristic measures from discrete data points, it is critical to create a smooth mathematical representation of the original anatomic structure. Several methods have been suggested in the past for the computational reconstruction of the mitral annulus from discrete data points. Linear interpolation has been widely used among clinical researchers to characterize the mitral annulus in humans and in animal models.[18,20,21,48] More sophisticated approaches use one-dimensional (1D) interpolating Hermitian finite elements[13] or Fourier series to approximate the mitral annulus from echo data.[36] An alternative method to reconstruct space curves that provides a variety of practical advantages is spline fitting. Splines are piecewise polynomial functions that are continuous to a desired degree and allow for an efficient computational implementation.[12]

In what follows we illustrate the design of a mathematical model of the mitral annulus based on piecewise cubic splines. This mathematical representation lends itself naturally into a precise quantification of displacement, strain, and curvature fields to characterize not only the clinical but also the mechanical features of the mitral annulus. Our representation is based on 55 high-resolution data sets acquired directly in the beating heart. From these, we create a comprehensive baseline characterization of mitral annular form and function, and discuss its clinical significance in view of optimizing surgical techniques and medical device design for mitral valve repair.

MATERIALS AND METHODS

Animal Experiments

All animals received humane care in compliance with the Principles of Laboratory Animals Care formulated by the National Academy of Sciences and published by the National Institutes of Health. This study was approved by the Stanford Medical Center Laboratory Research Animals Review Committee and conducted according to Stanford University policy.

Prior to data acquisition, we pre-medicated 55 adult, male Dorsett-hybrid sheep (49 ± 5 kg) intramuscularly with ketamine (27 mg/kg IM) for placement of a single peripheral intravenous line, anesthetized them with sodium thiopental (6.8 mg/kg IV), intubated them, and ventilated them mechanically with inhalational isoflurane (1.5–2.2%). For bradycardia and to control secretions, we gave glycopyrrolate (0.1 mg/kg IV) as needed.

Following a left thoractomy and under cardiopulmonary bypass and cardioplegic arrest, we surgically implanted 16 miniature radiopaque tantulum markers onto the mitral annulus. We placed markers at the two trigones, at the mid-septal annulus, at both commissures, and at the center of the lateral mitral annulus. To subdivide the annulus in approximately equidistant segments, we placed additional markers as illustrated in Fig. 1. Before weaning the animals off cardiopulmonary bypass, we closed the left atrium. For biplane videofluoroscopic imaging, we transferred the animals to the experimental catheterization laboratory 1–2 h after weaning them off of cardiopulmonary bypass. After acquiring the data set for a separate study, acute ischemia with 90s of LCx occlusion,[3] we recorded 3D marker coordinates in the beating heart at a sampling frequency of 60 Hz under open chest conditions in the right lateral decubitus position. In order to prevent ventricular fibrillation, we administered a loading dose of lidocaine (1 mg/kg IV) followed by a lidocaine infusion (1 mg/min) along with bretylium (75 mg IV) and magnesium (3 g IV). Using catheter micromanometer pressure transducers, we simultaneously recorded atrial, ventricular, and aortic pressures. Using a semi-automated image processing and digitization software developed in our laboratory,[39] we obtained four-dimensional (4D) coordinates $\chi_n(t)$ of the $n = 1,\ldots,16$ implanted markers offline from the acquired biplane images.

Spatial Approximation of the Annulus

To create a functional representation of the annulus in terms of the acquired marker coordinates $\boldsymbol{\chi}_n(t)$, we generated 16 piecewise cubic Hermitian splines $\mathbf{c}_n(s, t)$ parameterized in terms of the arc length at each discrete time point t.

$$\mathbf{c}(s,t) = \sum_{i=0}^{3} b_{i,3}(s)\boldsymbol{\beta}_i(t). \tag{1}$$

Herein, $b_{i,3}$ are the Bernstein polynomials of degree three,

$$b_{i,3} = \binom{3}{i} s^i [1-s]^{3-i}, \quad i = 0,\ldots,3 \tag{2}$$

specifically

$$\begin{array}{ll} b_{0,3} = -s^3 + 3s^2 - 3s + 1 & b_{1,3} = 3s^3 - 6s^2 + 3s \\ b_{3,3} = s_3 & b_{2,3} = -3s^3 + 3s^2 \end{array} \tag{3}$$

and $\boldsymbol{\beta}_i(t)$ are the corresponding Bernstein coefficients.

$$\begin{array}{ll} \boldsymbol{\beta}_0 = \mathbf{x}_0(t) & \boldsymbol{\beta}_1 = \mathbf{x}_0(t) + \mathbf{m}_0(t)/3 \\ \boldsymbol{\beta}_3 = \mathbf{x}_1(t) & \boldsymbol{\beta}_2 = \mathbf{x}_1(t) - \mathbf{m}_1(t)/3 \end{array} \tag{4}$$

The Bernstein coefficients are expressed in terms of the marker positions $\mathbf{x}_0$, $\mathbf{x}_1$ and slopes $\mathbf{m}_0$, $\mathbf{m}_1$ at the beginning and end point of each spline segment, respectively. For each discrete time point t, we determined these coefficients $\boldsymbol{\beta}_i(t)$ by solving the following discrete minimization problem.

$$\left| \sum_{n=1}^{16} \|\boldsymbol{\chi}_n - \mathbf{c}_n(s,t)\| + \lambda \int \left[\frac{d^2\mathbf{c}(s,t)}{ds^2}\right]^2 ds \right| \to \min \tag{5}$$

The first term $||\boldsymbol{\chi}_n - \mathbf{c}_n(s, t)||$ ensures that the 16 generated splines $\mathbf{c}_n(s, t)$ approximate the 16 marker positions $\boldsymbol{\chi}_n$ in the best possible way, while the second term enforces smoothness of the overall annulus representation through the penalty parameter λ. This procedure allowed us to generate a smooth piecewise cubic representation $\mathbf{c}_n(s, t)$ of all 55 annuli at discrete time points t throughout the cardiac cycle.

Temporal Interpolation of the Annulus

To generate an average representation of the mitral valve annulus,[36] we mapped all 55 experimental data sets into four time intervals between End Diastole (ED), End IsoVolumic Contraction (EIVC), End Systole (ES), and End IsoVolumic Relaxation (EIVR). We then performed a linear temporal interpolation between the raw data points to create temporally aligned data sets of geometric and hemodynamic data over a cardiac cycle. Using these averaged geometric data, we applied the method described in "Spatial Approximation of the Annulus" section to obtain a mathematical model of the averaged mitral annulus throughout the cardiac cycle. To illustrate potential future applications of this model, we created rapid prototypes of the averaged mitral annulus representation at characteristic hemodynamic time points based on Eq. (1).

Clinical Characterization

To characterize annular physiology, we extracted classical clinical metrics of annular form and function from the averaged spline representation. In particular, we computed the Septal–Lateral (SL) and Commissure–Commissure (CC) distances after

projecting the spline into a best-fit plane to prevent interdependence of these parameters. In this best-fit plane, we fitted an ellipse to the spline curve and calculated its eccentricity. In addition, we calculated the 3D annular perimeter as the line integral along the spline in terms of the arc-length parameters. We divided this perimeter into a septal and lateral section defined by the trigone marker coordinates (LT and RT, see Fig. 1). Furthermore, we computed the MAA from the same projected spline. As a measure for the non-planarity, we calculated the SH as the distance of the commissures to a plane through the mid-septal and mid-lateral sections of the annulus and equidistant to the anterior and posterior commissure. Finally, we calculated the annular velocity as the temporal derivative of the absolute displacement of the mitral annulus normal to the best-fit plane through the 16 marker coordinates (see Fig. 1).

Mechanical Characterization

To characterize annular dynamics, we calculated displacement,[24,28] strain,[4,44] and curvature[19,32] fields from the discrete annulus representations. Accordingly, we evaluated the first and second spatial derivatives of the spline curve (1) as:

$$\frac{d\mathbf{c}(s,t)}{ds} = \sum_{i=0}^{3} \frac{db_{i,3}(s)}{ds}\boldsymbol{\beta}_i(t) \tag{6}$$

in terms of the first derivatives of the Bernstein polynomials (3)

$$\begin{aligned} \frac{db_{0,3}}{ds} &= -2s^2 + 6s - 3 & \frac{db_{1,3}}{ds} &= 9s^2 - 12s + 3 \\ \frac{db_{3,3}}{ds} &= 3s^2 & \frac{db_{2,3}}{ds} &= -9s^2 + 6s \end{aligned} \tag{7}$$

and

$$\frac{d^2\mathbf{c}(s,t)}{ds^2} = \sum_{i=0}^{3} \frac{d^2b_{i,3}(s)}{ds^2}\boldsymbol{\beta}_i(t) \tag{8}$$

in terms of the second derivatives of the Bernstein polynomials (3).

$$\begin{aligned} \frac{d^2b_{0,3}}{ds^2} &= -4s + 6 & \frac{d^2b_{1,3}}{ds^2} &= 18s - 12 \\ \frac{d^2b_{3,3}}{ds^2} &= 6s & \frac{d^2b_{2,3}}{ds^2} &= -18s + 6 \end{aligned} \tag{9}$$

For each discrete time point t, we determined the best-fit plane through the approximated 16 marker points x_n. The unit normal to this plane defines the binormal vector, $\mathbf{b}(t)$, such that the local coordinate system at each point along the curve can be characterized through the triad [**t**, **n**, **b**] with

$$\mathbf{t}(s,t) = \frac{d\mathbf{c}(s,t)}{ds} \Big/ \left|\frac{d\mathbf{c}(s,t)}{ds}\right| \tag{10}$$

and

$$\mathbf{n}(s,t) = \mathbf{b}(t) \times \mathbf{t}(s,t) \tag{11}$$

Herein, **t** is the unit tangent vector, **n** is the unit normal vector, and **b** is the unit binormal vector to the curve **c** at point s and time t, see Fig. 1. The relative displacement of the annulus $\mathbf{c}(s, t)$ with respect to its reference position at minimum Left Ventricular Pressure ($\mathrm{LVP_{min}}$) $\mathbf{c}\left(s, t^{\mathrm{LVP_{min}}}\right)$ can be used to derive global indices for ventricular function. It is characterized through the discrete distance vector $\mathbf{u}(s, t)$

$$\mathbf{u}(s,t) = \mathbf{c}(s,t) - \mathbf{c}\left(s, t^{\mathrm{LVP_{min}}}\right) \tag{12}$$

projected onto the binormal vector $\mathbf{b}(t)$

$$u_b(s,t) = \mathbf{u}(s,t) \cdot \mathbf{b}(t) \tag{13}$$

for each point s along the curve at every discrete time point t. Next, we calculated the Green–Lagrange strain $E(s, t)$ along the annulus in terms of the stretch $\lambda(s, t)$,

$$E(s,t) = \frac{1}{2}\left[\lambda(s,t)^2 - 1\right] \tag{14}$$

with the stretch $\lambda(s, t)$

$$\lambda(s,t) = \left|\frac{d\mathbf{c}(s,t)}{ds}\right| \Big/ \left|\frac{d\mathbf{c}\left(s, t^{\mathrm{LVP_{min}}}\right)}{ds}\right| \tag{15}$$

characterizing the change in length between the tangent vector of the reference configuration at $\mathrm{LVP_{min}}$, $d\mathbf{c}(s, t^{\mathrm{LVP_{min}}})/ds$, and the current configuration at any other time point, $d\mathbf{c}(s, t)/ds$. Finally, we calculated the curvature $\kappa(s, t)$,

$$\kappa(s,t) = \frac{d\mathbf{c}(s,t)}{ds} \times \frac{d^2\mathbf{c}(s,t)}{ds^2} \Big/ \left|\frac{d\mathbf{c}(s,t)}{ds}^3\right| \tag{16}$$

along the annulus.

Statistical Analysis

We compared peak values for clinical metrics in diastole and systole using paired, two-tailed, two-sample Student t test with an alpha level of 0.05. To ensure normality, we plotted histograms of the data.

RESULTS

Clinical Characterization

Hemodynamic data of all 55 animals are summarized in Table 1. Figure 2 summarizes temporal and

TABLE 1. Summary of hemodynamic data of all 55 animals showing averages of Heart Rate (HR), Maximum Pressure Gradient (dP/dt_{max}), End Diastolic Volume (EDV), End Systolic Volume (ESV), Stroke Volume (SV), Left Ventricular End Diastolic Pressure (LVEDP), Left Ventricular End Systolic Pressure (LVESP), and Maximum Left Ventricular Pressure (LVP_{max}); ±Standard Deviations (SD).

	HR (beats/min)	dP/dt_{max} (mmHg/s)	EDV (cc)	ESV (cc)	SV (cc)	EF (–)	LVEDP (mmHg)	LVESP (mmHg)	LVP_{max} (mmHg)
Mean	91.13	1310.60	119.66	91.50	28.17	0.23	12.30	93.00	96.82
±SD	13.22	342.73	18.64	14.84	9.20	0.06	4.73	8.26	7.78

inter-subject variations of classical clinical metrics of mitral annular form and function. In the following, it is important to keep in mind that the minima and maxima in the graphs in Fig. 2 display "*peak average*" values, while the values reported in the text are the "*average peak*" values. Accordingly, minimum/maximum values of the temporal averages shown in the graphs may not be identical to the average minimum/maximum values discussed in the text. The in-plane characteristics of the mitral annulus are best described in terms of the Septal–Lateral (SL) and Commissure–Commissure (CC) distances. Their temporal averages are shown in Figs. 2a and 2b. Both distances clearly change during the cardiac cycle being largest during diastole and smallest during systole. The average maxima, i.e., the average of the maximum values for each animal, were 3.03 ± 0.24 and 3.85 ± 0.26 cm for SL and CC, respectively, while the average minima were 2.66 ± 0.23 and 3.64 ± 0.26 cm, giving rise to dynamic changes of SL of -12.06% and CC of -5.51%, both with respect to the diastolic state. Herein, the minus sign indicates a reduction from diastole to systole. The differences between the diastolic and systolic values for both SL and CC were statistically significant ($p < 0.001$ in both cases). The inequality of SL and CC is also reflected in the elliptic annular projection with eccentricity values larger than 0. Recall that perfect circles have an eccentricity of 0, while ellipses have eccentricity values between 0 and 1. The asymmetric reduction in SL and CC during systole causes the annulus to further deviate from a circular shape evident from the increase in eccentricity, Fig. 2c. The average minimum eccentricity during diastole was 0.61 ± 0.06, while the average maximum value during systole was 0.71 ± 0.04 a change throughout the cardiac cycle of $+13.5\%$. Again, values in diastole and systole were significantly different ($p < 0.001$). Furthermore, the decreases in SL and CC were accompanied by changes in the septal and lateral perimeters shown in Figs. 2d and 2e, respectively. The septal portion increased in perimeter from diastole to systole with average minima and maxima, respectively, of 1.43 ± 0.21 and 1.52 ± 0.22 cm giving rise to a relative change of $+6.0\%$ ($p < 0.05$). In contrast to the septal perimeter, the lateral perimeter behaved similar to SL and CC with an average maximum of 9.85 ± 0.61 cm during diastole, an average minimum of 9.17 ± 0.65 cm during systole (significantly different with $p < 0.001$), and a relative change of -6.9%. Changes in the above parameters cause the MAA to decrease from diastole to systole, see Fig. 2f. In addition, MAA decreased from an average maximum of 9.47 ± 1.15 cm^2 to an average minimum of 8.09 ± 1.12 cm^2 with an average maximum change of $+14.6\%$ ($p < 0.001$).

The out-of-plane characteristics of the mitral annulus are typically described in terms of the SH, see Fig. 2g. This study shows that the SH changes dynamically throughout the cardiac cycle with an average minimum during diastole of 0.20 ± 0.15 cm, an average maximum during systole of 0.33 ± 0.15 cm and an average change of $+65.0\%$ ($p < 0.001$). Lastly, Fig. 2h displays the dynamic motion of the mitral annulus normal to the best fit plane through the 16 marker coordinates. During diastole the annulus moves in the basal direction with average maximum velocities of up to 5.08 ± 1.42 cm s^{-1} During systole the contracting heart causes the annulus to accelerate in the apical direction with average maximum negative velocities of up to -3.11 ± 1.18 cm s^{-1} ($p < 0.001$).

Mechanical Characterization

Figure 3 displays the regional variation of averaged mitral annular kinematics at five characteristic time points throughout the cardiac cycle: minimum Left Ventricular Pressure (LVP_{min}), End Diastole (ED), End IsoVolumetric Contraction (EIVC), End Systole (ES), and End IsoVolumetric Relaxation (EIVR). The piecewise cubic spline approximated all experimentally acquired marker coordinates $\chi_n(t)$ extremely well with a maximum error at any time and any marker location of less than 0.07 cm. This value is on the order of the digitization error of 0.01 ± 0.03 cm of the marker technique.[4,19,32,44] Moreover, we observed no local maxima in curvature close to the original marker locations indicating a good choice for the smoothing parameter λ. Figure 3a illustrates the annular excursion of the mitral valve as a measure of left ventricular long-axis shortening,[25,43] displayed in an anterior view.

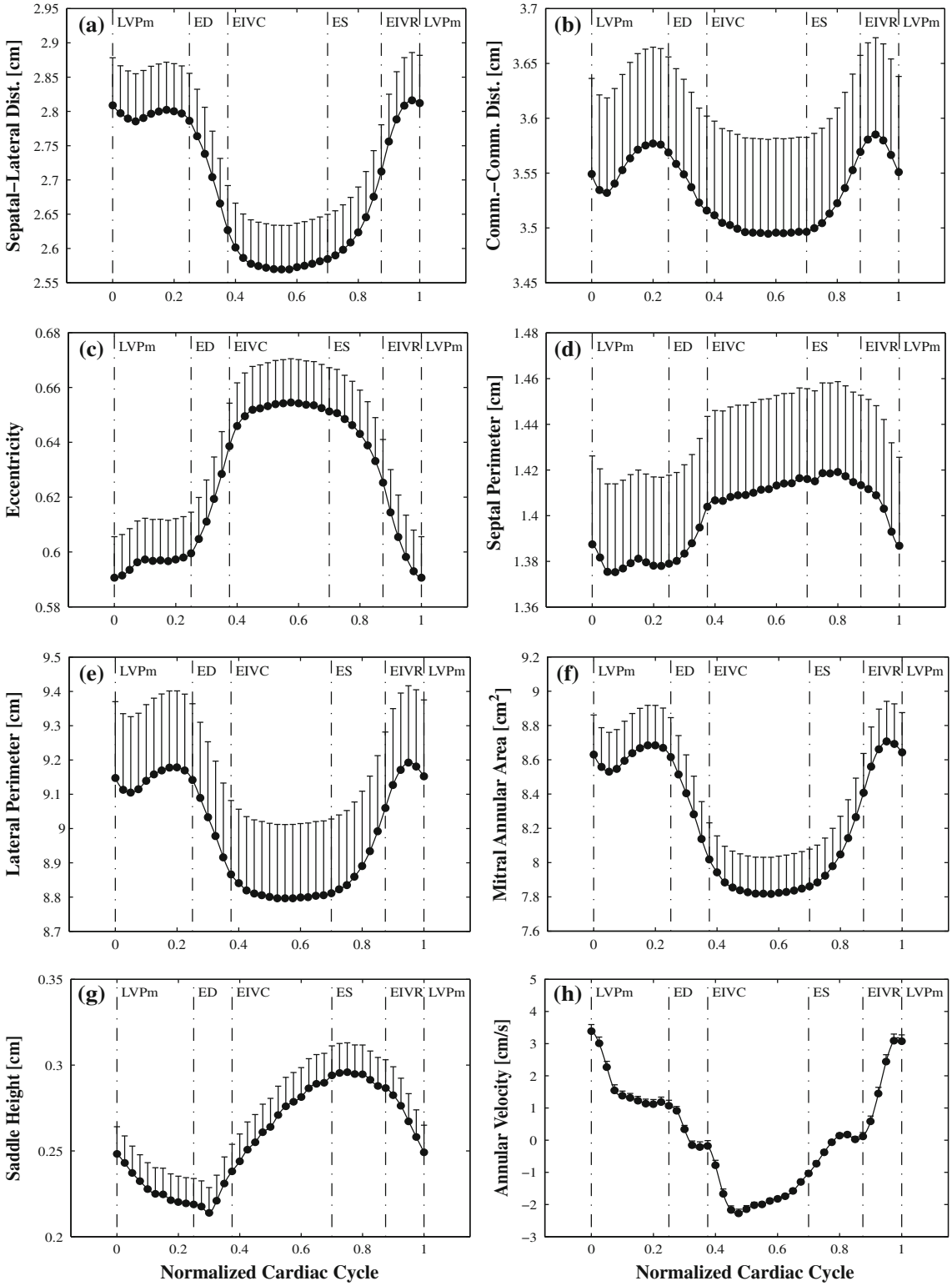

FIGURE 2. Clinical characterization of averaged mitral annulus throughout the cardiac cycle. Vertical lines indicate characteristic time points: minimum Left Ventricular Pressure (LVP_{min}), End Diastole (ED), End IsoVolumetric Contraction (EIVC), End Systole (ES), and End IsoVolumetric Relaxation (EIVR). Data are mean ± SEM for n = 55 annuli.

Clearly, the mitral annulus moves basally between LVP_{min} and the beginning of systole. In addition, the mid-septal annulus moves in the lateral direction. With progressing systole, the annulus returns back towards the apex, while the ventricular long-axis is shortening. Figure 3b illustrates the normal strains of the annulus

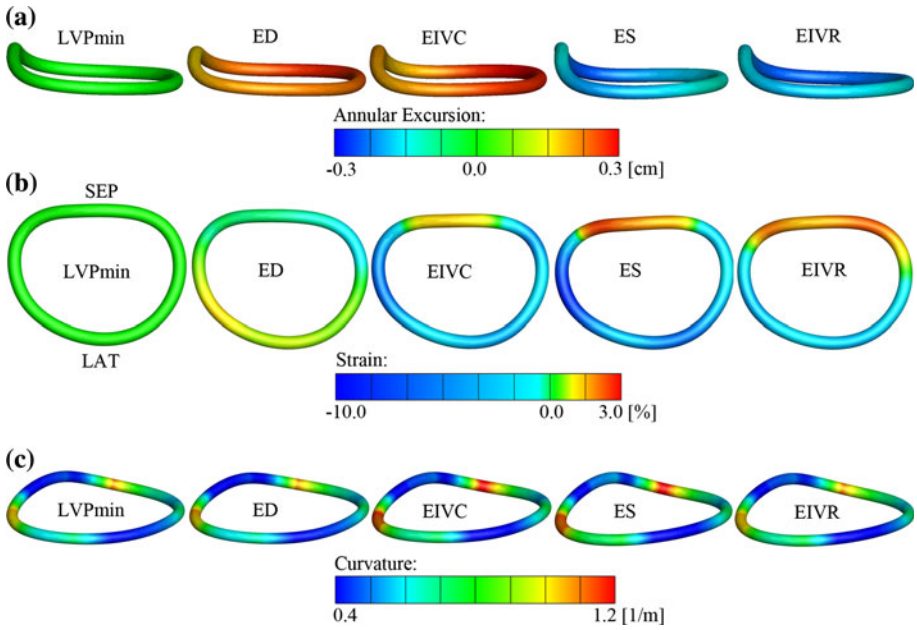

FIGURE 3. Regional variation of averaged mitral annular kinematics at five characteristic time points throughout the cardiac cycle: minimum Left Ventricular Pressure (LVP_{min}), End Diastole (ED), End IsoVolumetric Contraction (EIVC), End Systole (ES), and End IsoVolumetric Relaxation (EIVR). (a) Annular excursion as a measure of left ventricular long-axis shortening, displayed in anterior view. The color code represents the distance of the annulus along the long-axis of the left ventricle throughout the cardiac cycle relative to its position at LVP_{min}. Blue colors indicate displacements toward the apex, red colors represent displacements away from the apex. (b) Annular strains displayed in atrial view. The color code represents normal strains along the annulus between the current configuration and the reference configuration at LVP_{min}. Blue colors indicate compression, red colors indicate tension. (c) Annular curvature displayed in three-dimensional view. Curvature can be interpreted as the reciprocal of the radius of an inscribed sphere at any location. Blue colors indicate straighter segments and red colors indicate a higher degree of bending.

displayed in an atrial view. While strains toward ED display slightly positive values at the lateral portion, after the onset of systole strains are clearly compressive throughout the whole lateral perimeter with maximum values occurring toward the antero-lateral and postero-medial portions. In contrast, the septal portion displays negative strain values at ED and positive during systole meaning that the septal annulus is stretched rather than compressed as the lateral part. Figure 3c illustrates the annular curvature displayed in a 3D view. As apparent from the contour plots, the largest curvature values can be found at the transition region from the lateral to the septal annulus where the annulus curves into the mid-septal annulus. Points of minimum curvature appear to be at the central regions of both annular portions. Throughout the cardiac cycle, these patterns remain qualitatively identical.

Figure 4 displays the temporal variation of the averaged mitral annular kinematics throughout the cardiac cycle. Throughout the 40-time-frame sequence, strain profiles display two distinct patterns. During diastole, the largest compressive strain the septal annulus experiences on average is $-4.93 \pm 2.06\%$, while the largest tensile strain experienced by the lateral annulus on average is $11.23 \pm 4.92\%$. During systole, the largest tensile strain the septal annulus experiences on average is $6.27 \pm 3.05\%$, while the largest compressive strain experienced by the lateral annulus on average is $-14.83 \pm 3.82\%$.

Figure 5 displays the inter-subject variation of mitral annular strains calculated individually for all 55 annuli. LVP_{min} was chosen as reference configuration and ES as current configuration. The majority of the annuli experience maximum tensile strains in the septal region and maximum compressive strains in the lateral region which is in agreement with the averaged strain representation in Fig. 3b.

Videos of the regional and temporal evolution of averaged displacement, strain, and curvature fields are available as electronic supplements.

DISCUSSION

We have established a mathematical model of the mitral valve annulus that allows a precise qualitative and quantitative assessment of annular dynamics in the beating heart. In contrast to previous studies, the mitral annulus was characterized throughout the entire cardiac cycle in terms of classical clinical metrics such as SL, CC, MAA, SH, and AV, and classical mechanical metrics such as displacement, strain, and curvature. Our baseline data set based on 55 annuli, traced videofluoroscopically at a high temporal and

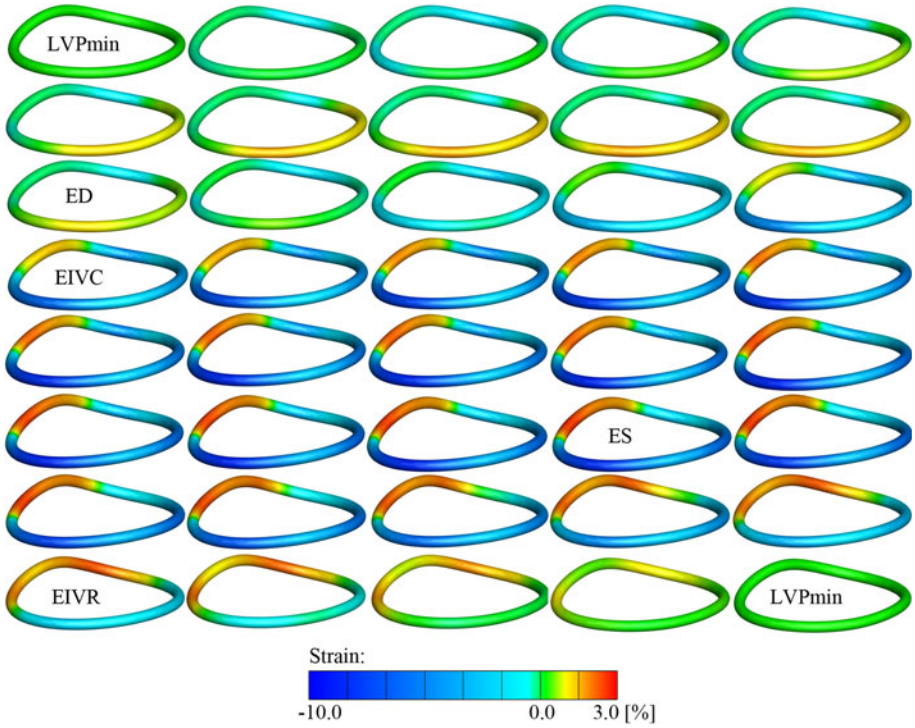

FIGURE 4. Temporal variation of averaged mitral annular kinematics throughout the cardiac cycle. The color code represents normal strains along the annulus between the current configuration and the reference configuration at minimum left ventricular pressure. Blue colors indicate compression, red colors indicate tension, and green color indicates no relative changes in length between the reference configuration and the current configuration. Strain profiles display two distinct patterns. During diastole, the entire annulus is virtually unstrained. During systole, the annulus experiences maximum tensile strains of 6.27 ± 3.05% in the septal region and maximum compressive strains of −14.83 ± 3.82% in the lateral region.

spatial resolution, allowed us to identify temporal, regional, and inter-subject variations of clinical and mechanical metrics to characterize mitral annular form and function.

Model Validation

Using the same imaging technique and the same animal model, Timek *et al.*[48] have previously applied line elements to reconstruct mitral annular geometry. They reported values closely resembling the findings here: MAA was 8.17 cm^2 at ED and 7.61 cm^2 at ES, slightly smaller than the 8.61 and 7.86 cm^2 that were derived from the smooth spline representation of the mitral annulus. Furthermore, they reported a total perimeter of 10.89 and 10.55 cm at ED and at ES, respectively, while the current study revealed 10.52 and 10.23 cm. In addition, SL and CC in Timek's study were 2.82 and 3.89 cm at ED, and 2.72 and 3.74 cm at ES. Similarly, in our study we found SL and CC to be 2.77 and 3.57 cm at ED, and 2.59 and 3.50 cm at ES. Differences are likely due to the smoothing character of the spline approximation that does not interpolate points but rather creates a best-fit curve, slightly reducing the perimeter, SL and CC, but increasing the enclosed area. Values for SH are similar to data reported by Gorman *et al.*[21] with 0.41 vs. 0.20 cm in our study at ED and 0.53 vs. 0.33 cm in our study at ES. Differences are likely due to the fact that different methods were used to compute SH.

Eckert *et al.*[13] previously reported strain and curvature in the ovine mitral annulus. Their peak strains in the septal and lateral regions are in excellent agreement with our findings both in systole and in diastole. However, their qualitative curvature plots display peak values at the mid-lateral portion and mid-septal portion where our study shows small values. From the steep gradient of their curvature profile around these points and from the proximity of curvature peaks to the original marker locations, it seems that their discrete annulus representation displays artificial discontinuities at these locations. The resulting curvature data are not intuitive from an engineering point of view and might be incorrect.

Clinical Significance

All current mitral valve reconstructive surgery techniques aim at restoring the native shape and competence of the mitral valve in order to re-establish normal

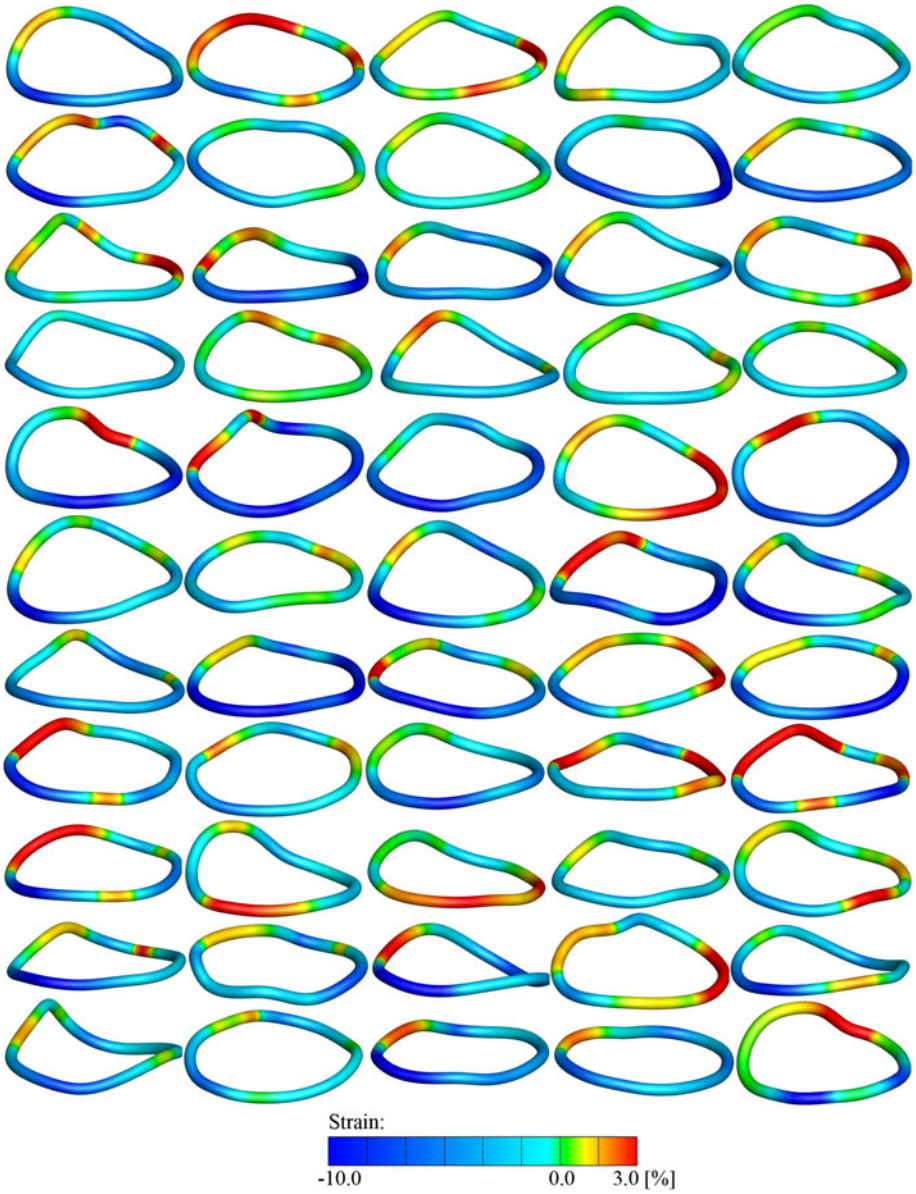

FIGURE 5. Inter-subject variation of mitral annular strains calculated individually for all 55 annuli. The color code represents normal strains along the annulus between the current configuration at End Systole (ES) and the reference configuration at minimum Left Ventricular Pressure (LVP_{min}). Blue colors indicate compression, red colors indicate tension, and green color indicates no relative changes in length between the reference configuration and the current configuration. The majority of the annuli experience maximum tensile strains in the septal region and maximum compressive strains in the lateral region.

cardiac function. The current study provides a comprehensive baseline data set for mitral annular dynamics in sheep. The 3D visualization of mitral annular motion, strains, and curvature in Figs. 3, 4, and 5 presents valuable information that will hopefully inspire further research in humans and thereby ultimately help the surgeon to characterize normal mitral annular form and function. In addition, novel reconstructive surgery techniques and medical device design might benefit from this high-resolution pool of information.

In contrast to most previously conducted investigations, our study not only provides a clinical characterization but also a mechanical characterization in terms of temporally and spatially varying kinematic fields. Strains were analyzed thoroughly along the perimeter over the entire range of motion. To identify potential risks of surgical techniques, it is important to keep in mind that large strain values indicate large relative changes in length. Such changes result from and cause large forces in the surrounding tissue both on the myocardial side and on the leaflet side. Suture lines placed close to highly strained mitral annular segments, for example, during anterior leaflet augmentation,[29] are therefore likely to experience large

stresses. Increased stresses in the mitral valve leaflets maybe associated with a higher risk of suture rupture that has been discussed as a potential causes for mitral valve repair failure.[45] This danger may be most prevalent during the first weeks post-operation as some evidence has been found that leaflet tissue, after several weeks, may form scar tissue around the suture lines providing the necessary mechanical strength to the leaflet and thereby prevent rupture.[47] Accordingly, the strain maps in Figs. 3, 4, and 5 may be useful to identify optimal suture locations to reduce repair failure. Furthermore, mitral annular segments such as the mid-portion of the lateral and septal annulus that show large absolute strain values are highly dynamic. Restriction of such dynamics, as seen upon annuloplasty ring implantation,[16] may disturb the natural force balance of the surrounding tissue and trigger a cascade of detrimental responses. Fixing the septal annulus during annuloplasty, for example, via the aorto-mitral junction may suppress the natural dynamics of the aortic root,[34] which has been shown to be crucial in minimizing shear stress on the aortic leaflets.[10] The strain maps along the perimeter of the mitral annulus as shown in Figs. 3 and 4 could therefore provide valuable guidelines to optimize repair techniques and device design.

At this point, it seems critical to draw attention to the large inter-subject variation of the strain patterns found among the 55 animals. Previous reports have either concentrated on reporting mean values to characterize the mechanics of the annulus or presented representative cases. The inter-subject variability illustrated in Fig. 5 may encourage the development of patient-specific devices and procedures to decrease the possibility of device and repair failures.[35]

To the best of our knowledge, this study is the first to correctly characterize mitral annular curvature in the beating heart. Remarkably, despite the highly dynamic character of the mitral annulus, Fig. 3c confirms that the curvature profile remains virtually unchanged throughout the cardiac cycle. This suggests that the particular curvature pattern of each annulus is advantageous in view of valve competence. Again, for annuloplasty rings that aim at mimicking the shape of the native annulus, our data set may provide a rational basis for an optimized ring design.

Mathematical Annulus Model as Interface with Engineering Technologies

In the past decades, the finite element analysis has become an important technology of many scientific disciplines including cardiac surgery.[31,50] However, numerical methods such as finite element analyses are highly sensitive to the choice of boundary conditions that, to a large extent, determine the results of the analysis and significantly impact the confidence in its outcome. Our mathematical model naturally characterizes both appropriate Dirichlet boundary conditions in terms of mitral annular shape and appropriate initial conditions in terms of mitral annular dynamics throughout the entire cardiac cycle.[30] Our data sets could be of particular interest to finite element modelers as the current trend in computational mitral valve analysis is moving toward developing more physiologically realistic models.[9,14,46,52]

With the tremendous development of rapid prototyping technologies, the process of creating prototypes has become cost effective and time inexpensive. The STL file format, which essentially approximates the surface of a solid with a finite number of discrete triangles, has become the interface of choice between computer-aided design and rapid prototyping. The proposed discrete spline representation $\mathbf{c}(s, t)$ of the mitral annulus given in Eq. (1) allows for a direct and straightforward extraction of STL files, as demonstrated in Fig. 6a. Our mathematical characterization of the mitral annulus therefore provides a direct interface between clinical data and state-of-the-art prototyping techniques. To demonstrate potential of our mathematical model, the averaged mitral annular geometry was used to manufacture subject-specific prototypes of a physiological annuloplasty ring at characteristic time points of the cardiac cycle.

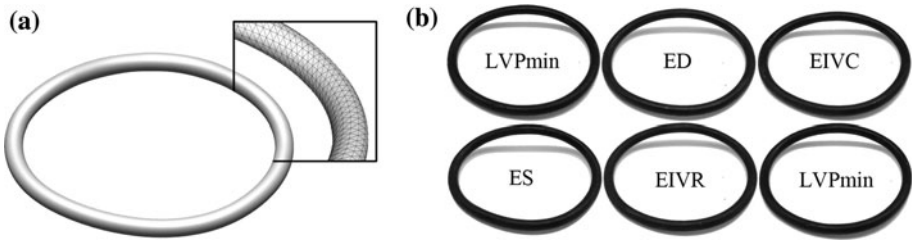

FIGURE 6. Averaged mitral annulus at five characteristic time points throughout the cardiac cycle: minimum Left Ventricular Pressure (LVP_{min}), End Diastole (ED), End IsoVolumetric Contraction (EIVC), End Systole (ES), and End IsoVolumetric Relaxation (EIVR). (a) Average mitral annulus at ES in STL file format. The STL file format approximates the surface of a solid model with discrete triangles. It was generated from the discrete spline representation c(*s*, *t*) of Eq. (1). (b) Photographs of rapid prototypes of the averaged mitral annulus at LVP_{min}, ED, EIVC, ES and EIVR manufactured directly from the STL file.

Photographs of these manufactured rings are illustrated in Fig. 6b.

Limitations

The mathematical model developed in the course of this study does not exactly represent the marker data collected during biplane videofluoroscopy. The underlying idea, however, is that the collected marker coordinates themselves contain an acquisition error, and that the anatomical structure represented through discrete data points is not curvature-discontinuous but rather smooth. We believe that a cubic spline approximation provides a better representation of the mitral annulus than discrete line elements or interpolations that force the representation to pass through discrete points which themselves might contain acquisition errors.

Second, it could generally be argued that marker implantation may impact annular motion and therefore affect mitral annular dynamics. Our implanted markers weighed 3.2 mg each and therefore had a cumulative weight of approximately 50 mg. During the relatively small acceleration of the mitral annulus, these small weights are not expected to produce significant additional inertial effects that could induce non-physiological dynamics.

Third, as a part of a different study, the 55 sheep underwent brief periods of less than 90s of acute ischemia before the marker coordinates were recorded. Together with the impact of the surgical procedure for marker placement, this may theoretically affect normal cardiac mechanics. For example, we observed that the sphincter motion of the annulus was delayed in comparison to earlier studies in our laboratory,[17] which could possibly be a result of the mentioned interventional procedures.

Finally, even though sheep have been recommended as large animal models for human cardiovascular disease and have been widely used in the past, their physiology and anatomy, after all, are different from human. Taken these differences and the fact that the sheep herein where studied after open heart surgery and under open chest conditions, the results presented herein must be used with caution and with the according limitations in mind when extrapolated to human hearts.

CONCLUSION

We have established a mathematical model of the mitral valve annulus that allows a precise qualitative and quantitative assessment of annular dynamics in the beating heart. Using this model, we have identified temporal, regional, and inter-subject variations of clinical and mechanical metrics to characterize mitral annular form and function. A quantitative mathematical model of mitral annular dynamics over the entire cardiac cycle has a plentitude of potential clinical implications some of which we have discussed in detail. It is our hope that this study will inspire similar studies in human subject employing non-invasive imaging techniques such as 3D echocardiography or MRI to eventually help identify regions of low strain as safe suture locations to reduce the risks of rupture and repair failure. To improve medical device design, our model can be used to create templates of subject-specific annuloplasty rings. We believe that our mathematical model will be useful to researchers, physicians, and ultimately patients. We hope that it will not only contribute to develop a deepened understanding of mitral valve dynamics, but also to motivate further efforts that will improve the lives of patients suffering from mitral valve disease.

ELECTRONIC SUPPLEMENTARY MATERIAL

The online version of this article (doi:10.1007/s10439-011-0272-y) contains supplementary material, which is available to authorized users.

ACKNOWLEDGMENTS

We thank Paul Chang, Eleazar P. Briones, Lauren R. Davis, and Kathy N. Vo for technical assistance, Maggie Brophy and Sigurd Hartnett for careful marker image digitization, and George T. Daughters III for computation of 4D data from biplane 2D marker coordinates. This work was supported in part by the US National Science Foundation grant CAREER award CMMI-0952021 to Ellen Kuhl, by US National Institutes of Health grants R01 HL29589 and R01 HL67025 to D. Craig Miller, by the Deutsche Herzstiftung, Frankfurt, Germany, Research Grant S/06/07 to Wolfgang Bothe, by the U.S.- Norway Fulbright Foundation, the Swedish Heart-Lung Foundation, and the Swedish Society for Medical Research to John-Peder Escobar Kvitting, and by the Western States Affiliate American Heart Association Fellowship to Julia C. Swanson.

REFERENCES

[1]Azencott, R., R. Glowinsky, J. He, R. H. W. Hoppe, A. Jajoo, A. Martynenko, S. Benzecry, S. H. Little, and W. A. Zoghbi. Diffeomorphic matching and dynamic deformable

surfaces in 3D medical imaging. *Comput. Methods Appl. Math.* 10:1–57, 2010.

[2]Bonow, R. O., B. A. Carabello, K. Chatterjee, A. C. de Leon, D. P. Faxon, M. D. Freed, W. H. Gaasch, B. W. Lytle, R. A. Nishimura, P. T. O'Gara, R. A. O'Rourke, C. M. Otto, P. M. Shah, J. S. Shanewise, S. C. Smith, A. K. Jacobs, C. D. Adams, J. L. Anderson, E. M. Antman, D. P. Faxon, V. Fuster, J. L. Halperin, L. F. Hiratzka, S. A. Hunt, B. W. Lytle, R. Nishimura, R. L. Page, B. Riegel, and A. C. C. Heart. ACC/AHA 2006 guidelines for the management of patients with valvular heart disease. *Circulation* 114:E84–E231, 2006.

[3]Bothe, W., J. P. Escobar Kvitting, E. H. Stephens, J. C. Swanson, N. B. Ingels, and D. C. Miller. Effects of annuloplasty ring implantation on regional mitral leaflet tenting area during acute myocardial ischemia. *J. Thorac. Cardiovasc. Surg.* 141:345–353, 2011.

[4]Bothe, W., E. Kuhl, J. P. Kvitting, M. K. Rausch, S. Goktepe, J. C. Swanson, N. B. Ingels, and D. C. Miller. Rigid, complete annuloplasty rings increase anterior mitral leaflet strains in the normal beating ovine heart (submitted).

[5]Bothe, W., J. P. Kvitting, J. C. Swanson, S. Goktepe, K. N. Vo, N. B. Ingels, and D. C. Miller. How do annuloplasty rings affect mitral leaflet dynamic motion? *Eur. J. Cardiothorac. Surg.* 38(3):340–349, 2010.

[6]Bothe, W., J. P. Kvitting, J. C. Swanson, S. Hartnett, N. B. Ingels, Jr., and D. C. Miller. Effects of different annuloplasty rings on anterior mitral leaflet dimensions. *J. Thorac. Cardiovasc. Surg.* 139:1114–1122, 2010.

[7]Carpentier, A. La valvuloplastie reconstitutive. Une nouvelle technique de valvuloplastie mitrale. *Presse Med.* 77:251–253, 1969.

[8]Carpentier, A. Cardiac valve surgery—the ''French correction''. *J. Thorac. Cardiovasc. Surg.* 86:323–337, 1983.

[9]Conti, C. A., E. Votta, A. Della Corte, L. Del Viscovo, C. Bancone, M. Cotrufo, and A. Redaelli. Dynamic finite element analysis of the aortic root from MRI-derived parameters. *Med. Eng. Phys.* 32:212–221, 2010.

[10]Dagum, P., G. R. Green, F. J. Nistal, G. T. Daughters, T. A. Timek, L. E. Foppiano, A. F. Bolger, N. B. Ingels, and D. C. Miller, Jr. Deformational dynamics of the aortic root: modes and physiologic determinants. *Circulation* 100:II54–II62, 1999.

[11]Dagum, P., T. A. Timek, G. R. Green, D. Lai, G. T. Daughters, D. H. Liang, M. Hayase, N. B. Ingels, Jr., and D. C. Miller. Coordinate-free analysis of mitral valve dynamics in normal and ischemic hearts. *Circulation* 102:III62–III69, 2000.

[12]de Boor, C. A Practical Guide to Splines. New York: Springer, 368 pp, 1978.

[13]Eckert, C. E., B. Zubiate, M. Vergnat, J. H. Gorman, III, R. C. Gorman, and M. S. Sacks. In vivo dynamic deformation of the mitral valve annulus. *Ann. Biomed. Eng.* 37:1757–1771, 2009.

[14]Einstein, D. R., F. Del Pin, X. M. Jiao, A. P. Kuprat, J. P. Carson, K. S. Kunzelman, R. P. Cochran, J. M. Guccione, and M. B. Ratcliffe. Fluid-structure interactions of the mitral valve and left heart: comprehensive strategies, past, present and future. *Int. J. Numer. Methods Biomed. Eng.* 26:348–380, 2010.

[15]Enriquez-Sarano, M., C. W. Akins, and A. Vahanian. Mitral regurgitation. *Lancet* 373:1382–1394, 2009.

[16]Glasson, J. R., G. R. Green, J. F. Nistal, P. Dagum, M. Komeda, G. T. Daughters, A. F. Bolger, L. E. Foppiano, N. B. Ingels, Jr., and D. C. Miller. Mitral annular size and shape in sheep with annuloplasty rings. *J. Thorac. Cardiovasc. Surg.* 117:302–309, 1999.

[17]Glasson, J. R., M. Komeda, G. T. Daughters, L. E. Foppiano, A. F. Bolger, T. L. Tye, N. B. Ingels, and C. Miller. Most ovine mitral annular three-dimensional size reduction occurs before ventricular systole and is abolished with ventricular pacing. *Circulation* 96:115–122, 1997.

[18]Glasson, J. R., M. K. Komeda, G. T. Daughters, M. A. Niczyporuk, A. F. Bolger, N. B. Ingels, and D. C. Miller. Three-dimensional regional dynamics of the normal mitral anulus during left ventricular ejection. *J. Thorac. Cardiovasc. Surg.* 111:574–585, 1996.

[19]Goktepe, S., W. Bothe, J. P. Kvitting, J. C. Swanson, N. B. Ingels, D. C. Miller, and E. Kuhl. Anterior mitral leaflet curvature in the beating ovine heart: a case study using videofluoroscopic markers and subdivision surfaces. *Biomech. Model. Mechanobiol.* 9:281–293, 2010.

[20]Gorman, III, J. H., K. B. Gupta, J. T. Streicher, R. C. Gorman, B. M. Jackson, M. B. Ratcliffe, D. K. Bogen, and L. H. Jr. Edmunds. Dynamic three-dimensional imaging of the mitral valve and left ventricle by rapid sonomicrometry array localization. *J. Thorac. Cardiovasc. Surg.* 112:712–726, 1996.

[21]Gorman, III, J. H., B. M. Jackson, Y. Enomoto, and R. C. Gorman. The effect of regional ischemia on mitral valve annular saddle shape. *Ann. Thorac. Surg.* 77:544–548, 2004.

[22]Jimenez, J. H., S. W. Liou, M. Padala, Z. He, M. Sacks, R. C. Gorman, J. H. Gorman, III, and A. P. Yoganathan. A saddle-shaped annulus reduces systolic strain on the central region of the mitral valve anterior leaflet. *J. Thorac. Cardiovasc. Surg.* 134:1562–1568, 2007.

[23]Jimenez, J. H., D. D. Soerensen, Z. M. He, S. Q. He, and A. P. Yoganathan. Effects of a saddle shaped annulus on mitral valve function and chordal force distribution: an in vitro study. *Ann. Biomed. Eng.* 31:1171–1181, 2003.

[24]Jimenez, J. H., D. D. Soerensen, Z. M. He, J. Ritchie, and A. P. Yoganathan. Mitral valve function and chordal force distribution using a flexible annulus model: an in vitro study. *Ann. Biomed. Eng.* 33:557–566, 2005.

[25]Jones, C. J., L. Raposo, and D. G. Gibson. Functional importance of the long axis dynamics of the human left ventricle. *Br. Heart J.* 63:215–220, 1990.

[26]Kaplan, S. R., G. Bashein, F. H. Sheehan, M. E. Legget, B. Munt, X. N. Li, M. Sivarajan, E. L. Bolson, M. Zeppa, M. Z. Arch, and R. W. Martin. Three-dimensional echocardiographic assessment of annular shape changes in the normal and regurgitant mitral valve. *Am. Heart J.* 139:378–387, 2000.

[27]Kheradvar, A., and M. Gharib. Influence of ventricular pressure drop on mitral annulus dynamics through the process of vortex ring formation. *Ann. Biomed. Eng.* 35:2050–2064, 2007.

[28]Kheradvar, A., and M. Gharib. On mitral valve dynamics and its connection to early diastolic flow. *Ann. Biomed. Eng.* 37:1–13, 2009.

[29]Kincaid, E. H., R. D. Riley, M. H. Hines, J. W. Hammon, and N. D. Kon. Anterior leaflet augmentation for ischemic mitral regurgitation. *Ann. Thorac. Surg.* 78:564–568, 2004; (discussion 568).

[30]Krishnamurthy, G., D. B. Ennis, A. Itoh, W. Bothe, J. C. Swanson, M. Karlsson, E. Kuhl, D. C. Miller, and N. B. Ingels Jr. Material properties of the ovine mitral valve anterior leaflet in vivo from inverse finite element analysis. *Am. J. Physiol. Heart Circ. Physiol.* 295:H1141–H1149, 2008.

[31]Kunzelman, K. S., M. S. Reimink, and R. P. Cochran. Flexible versus rigid ring annuloplasty for mitral valve annular dilatation: a finite element model. *J. Heart Valve Dis.* 7:108–116, 1998.

[32]Kvitting, J. P., W. Bothe, S. Goektepe, M. K. Rausch, J. C. Swanson, E. Kuhl, N. B. Ingels, and D. C. Miller. Anterior mitral leaflet curvature during the cardiac cycle in the normal ovine heart. *Circulation* 122:1683–1689, 2010.

[33]Kwan, J., T. Shiota, D. A. Agler, Z. B. Popovic, J. X. Qin, M. A. Gillinov, W. J. Stewart, D. M. Cosgrove, P. M. McCarthy, and J. D. Thomas. Geometric differences of the mitral apparatus between ischemic and dilated cardiomyopathy with significant mitral regurgitation: real-time three-dimensional echocardiography study. *Circulation* 107:1135–1140, 2003.

[34]Lansac, E., K. H. Lim, Y. Shomura, W. A. Goetz, H. S. Lim, N. T. Rice, H. Saber, and C. M. Duran. Dynamic balance of the aortomitral junction. *J. Thorac. Cardiovasc. Surg.* 123:911–918, 2002.

[35]Lantada, A. D., R. Del Valle-Fernandez, P. L. Morgado, J. Munoz-Garcia, J. L. M. Sanz, J. M. Munoz-Guijosa, and J. E. Otero. Development of personalized annuloplasty rings: combination of ct images and CAD-CAM tools. *Ann. Biomed. Eng.* 38:280–290, 2010.

[36]Legget, M. E., G. Bashein, J. A. McDonald, B. I. Munt, R. W. Martin, C. M. Otto, and F. H. Sheehan. Three-dimensional measurement of the mitral annulus by multiplane transesophageal echocardiography: in vitro validation and in vivo demonstration. *J. Am. Soc. Echocardiogr.* 11:188–200, 1998.

[37]Levine, R. A., M. D. Handschumacher, A. J. Sanfilippo, A. A. Hagege, P. Harrigan, J. E. Marshall, and A. E. Weyman. Three-dimensional echocardiographic reconstruction of the mitral valve, with implications for the diagnosis of mitral valve prolapse. *Circulation* 80:589–598, 1989.

[38]Levine, R. A., M. O. Triulzi, P. Harrigan, and A. E. Weyman. The relationship of mitral annular shape to the diagnosis of mitral valve prolapse. *Circulation* 75:756–767, 1987.

[39]Niczyporuk, M. A., and D. C. Miller. Automatic tracking and digitization of multiple radiopaque myocardial markers. *Comput. Biomed. Res.* 24:129–142, 1991.

[40]Oliveira, J. M., and M. J. Antunes. Mitral valve repair: better than replacement. *Heart* 92:275–281, 2006.

[41]Ormiston, J. A., P. M. Shah, C. Tei, and M. Wong. Size and motion of the mitral valve annulus in man. I. A two-dimensional echocardiographic method and findings in normal subjects. *Circulation* 64:113–120, 1981.

[42]Padala, M., R. A. Hutchison, L. R. Croft, J. H. Jimenez, R. C. Gorman, J. H. Gorman, III, M. S. Sacks, and A. P. Yoganathan. Saddle shape of the mitral annulus reduces systolic strains on the P2 segment of the posterior mitral leaflet. *Ann. Thorac. Surg.* 88:1499–1504, 2009.

[43]Pai, R. G., M. M. Bodenheimer, S. M. Pai, J. H. Koss, and R. D. Adamick. Usefulness of systolic excursion of the mitral anulus as an index of left ventricular systolic function. *Am. J. Cardiol.* 67:222–224, 1991.

[44]Rausch, M. K., W. Bothe, J. P. Kvitting, S. Goektepe, D. C. Miller, and E. Kuhl. In vivo dynamic strains of the entire ovine anterior mitral valve leaflet. *J. Biomech.* 2011. doi:10.1016/j.jbiomech.2011.01.020.

[45]Salgo, I. S., J. H. Gorman, III, R. C. Gorman, B. M. Jackson, F. W. Bowen, T. Plappert, M. G. St John Sutton, L. H. Edmunds Jr., *et al.* Effect of annular shape on leaflet curvature in reducing mitral leaflet stress. *Circulation* 106:711–717, 2002.

[46]Stevanella, M., E. Votta, and A. Redaelli. Mitral valve finite element modeling: implications of tissues' nonlinear response and annular motion. *J. Biomech. Eng. Trans. ASME* 131:121010-1–121010-9, 2009.

[47]Tamura, K., M. Murakami, and M. Washizu. Healing of wound sutures on the mitral valve: an experimental study. *Gen. Thorac. Cardiovasc. Surg.* 55:98–104, 2007.

[48]Timek, T. A., P. Dagum, D. T. Lai, D. Liang, G. T. Daughters, F. Tibayan, N. B. Ingels, Jr., and D. C. Miller. Tachycardia-induced cardiomyopathy in the ovine heart: mitral annular dynamic three-dimensional geometry. *J. Thorac. Cardiovasc. Surg.* 125:315–324, 2003.

[49]Tsakiris, A. G., G. Von Bernuth, G. C. Rastelli, M. J. Bourgeois, J. L. Titus, and E. H. Wood. Size and motion of the mitral valve annulus in anesthetized intact dogs. *J. Appl. Physiol.* 30:611–618, 1971.

[50]Votta, E., F. Maisano, M. Soncini, A. Redaelli, F. M. Montevecchi, and O. Alfieri. 3-D computational analysis of the stress distribution on the leaflets after edge-to-edge repair of mitral regurgitation. *J. Heart Valve Dis.* 11:810–822, 2002.

[51]Watanabe, N., Y. Ogasawara, Y. Yamaura, N. Wada, T. Kawamoto, E. Toyota, T. Akasaka, and K. Yoshida. Mitral annulus flattens in ischemic mitral regurgitation: geometric differences between inferior and anterior myocardial infarction: a real-time 3-dimensional echocardiographic study. *Circulation* 112:I458–I462, 2005.

[52]Wenk, J. F., Z. H. Zhang, G. M. Cheng, D. Malhotra, G. Acevedo-Bolton, M. Burger, T. Suzuki, D. A. Saloner, A. W. Wallace, J. M. Guccione, and M. B. Ratcliffe. First finite element model of the left ventricle with mitral valve: insights into ischemic mitral regurgitation. *Ann. Thorac. Surg.* 89:1546–1554, 2010.